

RadCLIP: Enhancing Radiologic Image Analysis through Contrastive Language-Image Pre-training

Zhixiu Lu¹, Hailong Li^{1,2}, and Lili He^{1,2}

¹ Imaging Research Center, Department of Radiology,
Cincinnati Children's Hospital Medical Center

² Department of Radiology, University of Cincinnati College of Medicine

Abstract. The integration of artificial intelligence (AI) with radiology has marked a transformative era in medical diagnostics. Vision foundation models have been adopted to enhance radiologic imaging analysis. However, the distinct complexities of radiological imaging, including the interpretation of 2D and 3D radiological data, pose unique challenges that existing models, trained on general non-medical images, fail to address adequately. To bridge this gap and capitalize on the diagnostic precision required in medical imaging, we introduce RadCLIP: a pioneering cross-modal foundational model that harnesses Contrastive Language-Image Pre-training (CLIP) to refine radiologic image analysis. RadCLIP incorporates a novel 3D slice pooling mechanism tailored for volumetric image analysis and is trained using a comprehensive and diverse dataset of radiologic image-text pairs. Our evaluations demonstrate that RadCLIP effectively aligns radiological images with their corresponding textual annotations, and in the meantime, offers a robust vision backbone for radiologic imagery with significant promise.

Keywords: Radiology, Foundation Model, Vision-Language Pretraining, Diagnostics

1. Introduction

In the rapidly evolving field of radiology, the integration of artificial intelligence (AI) has become indispensable. Vision foundation models, trained on extensive datasets to learn a wide array of features, have shown exceptional promise in computer vision [1]. These models serve as a cornerstone for developing specialized applications, particularly through transfer learning, where knowledge from a source domain is applied to enhance performance in target domain. In medical imaging domain, the importance of transfer learning is further highlighted due to the difficulty of acquiring large datasets to train an end-to-end deep-learning model from scratch [2,3].

1.1 Need for Radiologic Image Foundation Models

State of the art (SOTA) vision foundation models are generally trained on natural image datasets, such as Cifar10, fodd101 and ImageNet [4,5]. However, the unique challenges of radiologic imaging data, such as 2D/3D attributes of radiological images, the subtlety of pathological features, and the high stakes of diagnostic accuracy, demand foundation models tailored to the medical domain. Generic vision models trained on natural image datasets may not capture the intricacies of radiological images, leading to a gap in performance when applied to clinical image classification tasks [6].

1.2 Vision-Language Models

Recent advances in vision-language models have significantly narrowed the gap between visual and textual information. The pioneering work by OpenAI with the Contrastive Language-Image Pre-training (CLIP) [1] leverages extensive image-text datasets for effective visual-textual concept association, enabling diverse applications like zero-shot image recognition and advanced natural language tasks. Its adaptability and robustness underscore its foundational role in the field. Alongside CLIP, models such as CoCa [7] and BLIP [8] have pushed the boundaries in cross-modal tasks and set new standards in vision benchmarks, showcasing the potential of vision-language pretraining (VLP) to enhance vision models through language supervision.

1.3 Medical Vision Language Models

Recently, there has been a surge in initiatives to tailor vision-language models for the medical domain, with several noteworthy projects emerging:

CONVIRT [9] automates radiology report generation through natural language processing, streamlining the interpretation process.

GLoRIA [10] leverages radiology reports to enhance medical image analysis without extensive labeling, using attention mechanisms to improve diagnostics in retrieval, classification, and segmentation.

MedCLIP [11] uses the CLIP framework on chest X-rays to link images with clinical notes, boosting diagnostic accuracy through zero-shot learning.

PMC-CLIP [12] extracts information from medical literature to facilitate its application in clinical settings.

CLIP-Lung [13] combines clinical text annotations with image data to better predict 3D CT lung nodule malignancy through channel-wise condition prompting, being one of the few methods attempting to extend VLP to 3D radiologic data.

CXR-CLIP [14] addresses chest X-ray data scarcity by merging image-text and image-label data, introducing novel contrastive losses for expanded training data diversity and learning study-level characteristics.

1.4 Limitations of Existing Medical VLP Models

Current proposed VLP models underscore potentials of vision-language approaches in radiologic imaging, yet they share a few common limitations RadCLIP aims to address:

Lack of diverse radiologic training data: One significant limitation is the lack of extensive and diverse radiologic training data for training and validation. Most existing models are often restricted to chest X-rays or slices of CT scan. The absence of data diversity limits the models' ability to generalize across imaging modalities.

Limited to 2D Imaging: Furthermore, these models generally do not possess the capability to process 3D radiological data, a critical component in many medical imaging modalities, such as CT and MRI. This significantly limits their applicability in scenarios where 3D spatial information is crucial for accurate diagnosis and assessment of medical conditions.

1.5 Motivation

We introduce RadCLIP, a novel VLP foundational model tailored for radiological image analysis. RadCLIP is designed to overcome the limitations of existing models with a focus on improving radiologic image representation learning. Utilizing a diverse, carefully curated radiologic dataset, we build a robust vision backbone for radiological imaging and enhance its cross-modal capabilities through vision-language pretraining. We aim to evaluate the performance of the proposed RadCLIP model on both unimodal radiologic image representation learning and cross-modal vision-language alignment.

1.6 Contribution

Overall, we make the following contributions in this study: **First**, we propose a joint framework to apply vision-language pretraining for both 2D and 3D radiological images. **Second**, we train the model using a carefully curated, diverse radiologic image-text pair datasets across a wide range of radiologic imaging modalities, anatomical regions, diseases, and conditions. **Third**, our evaluation shows that trained RadCLIP model exhibits impressive unimodal representation learning capabilities for radiologic images, showing promising potential as a strong radiologic vision backbone.

2 Method

2.1 Model Architecture

RadCLIP's model structure is built upon the CLIP framework for radiological image by integrating a fine-tuned 2D vision encoder (**Fig. 1**) and an innovative slice pooling module designed for learning volumetric images (**Fig. 2**). The 2D vision encoder, leveraging CLIP's pre-trained weights, is fine-tuned using radiology-specific image-text

pairs, while the text encoder's weights are kept static. This strategy preserves the sophisticated language understanding capabilities of original CLIP model, ensuring that the vision encoder focuses solely on improving radiological image representations for more accurate image-text alignment.

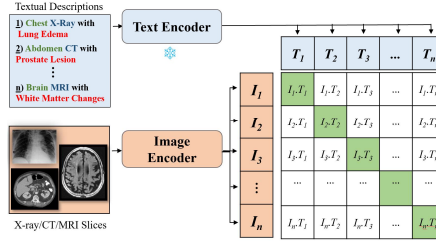


Fig. 1. Illustration of RadCLIP’s 2D module pre-training

For volumetric 3D radiologic images, data sparsity and complexity pose significant challenges for deep learning applications. Traditional methods commonly use either multi-channel feature maps or a pooling strategy for transition from 2D slice representations to 3D volume representation [13,21]. In the domain of video classification and annotation, approaches leveraging 2D image backbones to extract frame-wise representations and pool them into a single unified video representation have been largely successful [19,20]. In the medical domain, previous work such as COVID-VIT [17] has shown that similar approaches generalize well into volumetric image domain.

Inspired by these works, RadCLIP’s slice pooling module, as shown in Fig. 2, adopts an attention-based pooling mechanism to combine slice-wise 2D image representation based on their diagnostic importance and spatial position using multi-head self-attention and position encoding [22, 23]. This unified volume embeddings then undergoes same vision-language pre-training using volumetric image-text pairs to learn the detailed anatomy and pathology present in whole radiological volumes.

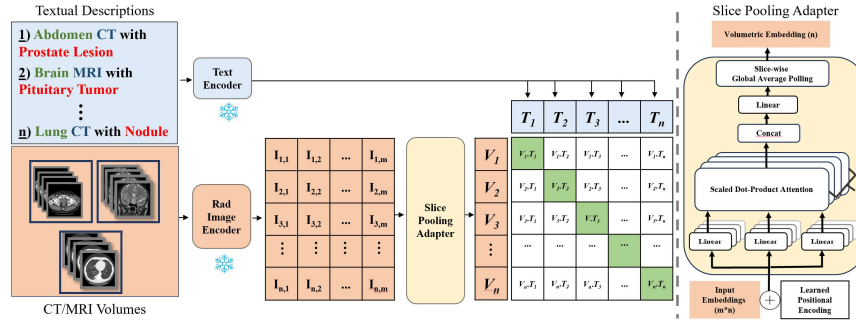


Fig. 2. Fig. 3 Left: Illustration of RadCLIP’s 3D model architecture. Right: Model architecture of the slice pooling adapter

2.2 Loss Function

To effectively align image and text representations within a shared embedding space, we leverage **Symmetric Contrastive Loss** to enhance the alignment of embeddings from images and texts, within a shared embedding space. This loss function employs a bidirectional approach to minimize the distance between semantically similar image-text pairs and maximize the distance between dissimilar ones. The core of the Symmetric Contrastive Loss lies in its computation of cosine similarity between image-text pairs. This scaling adjusts the distribution's concentration, affecting the degree separation between positive and negative examples. The similarity scores are calculated as:

$$\text{logits}_{ij} = \frac{\bar{v}_i \cdot \bar{t}_j}{\tau} \quad (1)$$

In a batch of N pairs, a similarity matrix is generated with positive examples (matching image-text pairs) along its diagonal and negative examples (non-matching pairs) elsewhere. The contrastive loss further introduces a symmetric approach by calculating the cross-entropy loss twice: once with images as anchors (loss_i), formulated as:

$$\text{loss}_i = -\frac{1}{N} \sum_{i=1}^N \log \left(\frac{\exp(\text{logits}_{ii})}{\sum_{j=1}^N \exp(\text{logits}_{ij})} \right) \quad (2)$$

and once with texts as anchors (loss_t), similarly formulated as

$$\text{loss}_t = -\frac{1}{N} \sum_{j=1}^N \log \left(\frac{\exp(\text{logits}_{jj})}{\sum_{i=1}^N \exp(\text{logits}_{ji})} \right) \quad (3)$$

And the final loss is simply the average of the two losses:

$$L = \frac{\text{loss}_i + \text{loss}_t}{2} \quad (4)$$

2.3 Implementation Details

For the basic CLIP architecture, we adopt ‘‘clip-vit-large-patch14’’ model published by OpenAI, the attention pooling module uses 4 attention heads and a learned positional encoding [23], both 2D and 3D modules are trained using AdamW optimizer with learning rate of 1e-4. The model is trained on 4*A6000 Nvidia GPU for a total of 32 hours. Model weights, training and evaluation codes will be made publicly available on Huggingface and GitHub upon acceptance.

3 Experiments

3.1 Dataset

To ensure that RadCLIP can understand a wide range of radiologic images, we curated a sizable radiology image dataset from publicly available radiologic image datasets for model pre-training, referred to as RadCLIP dataset. (**Fig. 4**) We include a total of 1,145,125 radiologic image-text pairs (2D X-ray, CT, and MRI images) and 62,257 radiologic 3D volume-text pairs (3D CT and MRI images). RadCLIP dataset covers a broad range of imaging sequences such as X-rays, CT scans, and MRI slices, across various anatomical sites including brain, chest, spine, abdomen, and extremities, among others, and a wide range of diseases and conditions within each category. Illustration of dataset is shown in figure 3 for 2D dataset.

	Anatomy	# Classes	Average class size	Total # image
X-ray	Chest	13	8,548	111,124
	Knee	4	40	160
	Spine	11	27	301
	Others	16	145	2,325
	Abdomen	33	4,917	162,270
CT	Chest	7	1,561	10,933
	Hand	1	10,000	10,000
	Head	1	10,000	10,000
	Lung	6	25,421	152,528
	Spine	1	472	472
	Abdomen	26	5,529	143,755
MRI	Ankle-Foot	25	14,446	361,158
	Brain	15	3,203	48,054
	Breast	1	8,954	8,954
	Hip	14	3,672	51,417
	Spine	9	7,963	71,674

Fig. 4. Illustration of RadCLIP dataset compilation

We also include 5 external evaluation datasets: chestXpert 5*1000 [11,28], CT-Abd-KAG, Crystal Clear Brain Tumor, OrganMNIST [29] and IXI Brain datasets. These datasets serve as hold out evaluations and are not involved in the training process. Detailed compilation of training and evaluation datasets and their sources are included in supplemental materials.

3.2 Linear Probing Classification

To evaluate RadCLIP’s unimodal performance as a standalone backbone vision encoder, we employ a widely recognized evaluation technique termed linear probing, as detailed in prior research [24]. This process involves fitting a single-layer linear classifier atop the foundational model’s generated features. This is utilized to benchmark performance across various classification tasks. Although an alternative method, model

fine-tuning, often leads to improved results, linear probing is a more robust and straightforward method for evaluating encoders’ representation learning efficacy [1,25].

We benchmark our RadCLIP along with four pretrained vision foundation models: ResNet50, Vision Transformer (ViT) [26], ViT-CLIP [1] and Swin Transformer (SwinT) [27]. These models are well known and widely adopted as vision backbones in various computer vision tasks, including those in the medical imaging domain.

In our evaluation, we train a single-layer classifier to classify representations generated by each vision encoder for 100 epochs using Adam optimizer at a learning rate of $1e-3$. We employ a 5-fold cross-validation, in which data is split into 70% training, 10% validation, and 20% testing during each iteration. Accuracy and F1 scores are calculated and averaged across folds, the results are included in table 1.

Model Name	ChestXpert (5 Classes, 2D)		CT-Abd-KAG (9 Classes, 2D)		Cystal Clear (4 Classes, 2D)		Organ MNIST (11 Classes, 3D)		IXI Brain (2 Classes, 3D)	
	Acc (%)	F1 (%)	Acc (%)	F1 (%)	Acc (%)	F1 (%)	Acc (%)	F1 (%)	Acc (%)	F1 (%)
ResNet50	41.98 (1.16)	41.74 (4.20)	96.03 (4.72)	93.71 (20.45)	63.00 (14.00)	60.04 (25.94)	70.26 (7.23)	78.32 (5.14)	68.49 (16.13)	72.41 (19.11)
SwinT	44.48 (1.27)	44.27 (5.60)	99.93 (0.14)	99.93 (0.34)	68.00 (7.48)	66.30 (19.33)	73.45 (6.27)	80.10 (4.16)	70.08 (5.92)	69.20 (14.95)
ViT	45.02 (1.97)	44.80 (5.51)	99.64 (0.32)	99.64 (0.81)	64.00 (5.83)	62.80 (15.27)	72.25 (6.19)	77.42 (5.09)	71.15 (6.34)	71.96 (8.52)
ViT-CLIP	41.44 (2.23)	40.44 (9.54)	95.37 (9.25)	93.61 (20.89)	71.00 (5.83)	73.13 (15.65)	69.65 (12.30)	71.84 (10.97)	74.33 (5.59)	72.18 (10.12)
ViT-RadCLIP	51.46 (1.32)	51.54 (5.15)	99.43 (0.58)	99.43 (1.11)	86.00 (3.74)	87.11 (10.01)	75.65 (5.31)	81.41 (4.07)	77.65 (4.53)	76.82 (5.32)

Table 1. Classification Results for RadCLIP

3.3 Image-Text Matching

To assess RadCLIP’s cross-modal proficiency in the radiology domain, we devise a simple, intuitive task: given a radiologic image, can RadCLIP accurately match it to corresponding text that describe anatomical regions and imaging modalities? We include three anatomical regions (chest, abdomen, brain) and three imaging modalities (X-ray, CT, MRI) in this experiment, resulting in 9 combinations of regions and modalities. Our analysis strictly utilizes external datasets. For 3D-level results, we use the same global pooling average for peer models for 2D-to-3D adaptation. The results are presented in Table 2.

Table 2. Top 1 accuracy of radiologic image-text matching

Model Name	ChestXpert (2D)	CT-Abd-KAG (2D)	Cystal Clear (2D)	OrganMNIST (3D)	IXI Brain (3D)
CLIP	99.74%	43.04%	74.87%	99.60%	95.58%
PMC-CLIP	99.48%	84.30%	93.44%	99.46%	96.28%
RadCLIP	99.98%	79.62%	99.77%	99.46%	98.76%

The evaluation of RadCLIP across linear probing and image-text matching tasks demonstrates its proficiency in both unimodal and cross-modal contexts for radiologic images. Through linear probing, RadCLIP exhibits impressive representation learning capability on radiologic images, underscore its robustness and potential for deep learning applications in the domain of medical images. Meanwhile, RadCLIP’s image text matching results demonstrate formidable cross-modal understanding between radiologic images and texts.

4 Limitations

4.1 Unknow performance on unseen data modalities

RadCLIP shows promising potential in its strong representation learning capability in radiologic imaging domain. However, despite efforts to include a wide range of radiologic imaging modalities, our study only encompasses X-ray, CT, and MRI images. Other imaging types like ultrasound, PET scans, and endoscopic images are excluded due to challenges in gathering a large and diverse dataset, leaving the model’s performance on these unrepresented modalities uncertain.

4.2 Constrained 3D Performance

Our proposed slice pooling module, although making it feasible to create a meaningful and unified representation for 3D volumetric images, relies heavily on the 2D backbone vision model’s representation learning capability. Our 3D dataset is significantly smaller and less diverse than 2D datasets used for training.

5 Conclusion

Here, we introduce RadCLIP, a novel vision-language foundation model designed to enhance radiologic image analysis through contrastive language-image pre-training. Our experiments demonstrate that RadCLIP can significantly improve upon existing vision foundation models by providing a stronger vision backbone in the domain of medical imaging. Furthermore, we propose a novel parameter-efficient slice pooling module that efficiently transfers learned 2D slice representations into a unified 3D volumetric representation, extending CLIP style vision-language pretraining approaches to essential radiologic volumetric imaging data.

References

1. A. Radford *et al.*, “Learning Transferable Visual Models From Natural Language Supervision,” *arXiv.org*, Feb. 26, 2021. <https://arxiv.org/abs/2103.00020>
2. H. E. Kim, A. Cosa-Linan, N. Santhanam, M. Jannesari, M. E. Maros, and T. Ganslandt, “Transfer learning for medical image classification: a literature review,” *BMC Medical Imaging*, vol. 22, no. 1, pp. 1–13, Apr. 2022, doi: 10.1186/s12880-022-00793-7.
3. C. M. J. F. H. M. S. M. S. K. Smith, “What Makes Transfer Learning Work for Medical Images: Feature Reuse & Other Factors”.
4. K. He, X. Zhang, S. Ren, and J. Sun, “Deep Residual Learning for Image Recognition,” *arXiv.org*, Dec. 10, 2015. <https://arxiv.org/abs/1512.03385>
5. A. Dosovitskiy *et al.*, “An Image is Worth 16x16 Words: Transformers for Image Recognition at Scale,” *arXiv.org*, Oct. 22, 2020. <https://arxiv.org/abs/2010.11929>
6. X. Mei *et al.*, “RadImageNet: An Open Radiologic Deep Learning Research Dataset for Effective Transfer Learning,” *Radiology: Artificial Intelligence*, vol. 4, no. 5, Sep. 2022, doi: 10.1148/ryai.210315.
7. J. Yu, Z. Wang, V. Vasudevan, L. Yeung, M. Seyedhosseini, and Y. Wu, “CoCa: Contrastive Captioners are Image-Text Foundation Models,” *arXiv.org*, May 04, 2022. <https://arxiv.org/abs/2205.01917>
8. J. Li, D. Li, C. Xiong, and S. Hoi, “BLIP: Bootstrapping Language-Image Pre-training for Unified Vision-Language Understanding and Generation,” *arXiv.org*, Jan. 28, 2022. <https://arxiv.org/abs/2201.12086>
9. Y. Zhang, H. Jiang, Y. Miura, C. D. Manning, and C. P. Langlotz, “Contrastive Learning of Medical Visual Representations from Paired Images and Text,” *arXiv.org*, Oct. 02, 2020. <https://arxiv.org/abs/2010.00747>
10. S.-C. H. L. S. M. P. L. S. Yeung, “GLoRIA: A Multimodal Global-Local Representation Learning Framework for Label-Efficient Medical Image Recognition”.
11. Z. Wang, Z. Wu, D. Agarwal, and J. Sun, “MedCLIP: Contrastive Learning from Unpaired Medical Images and Text,” in *Proceedings of the 2022 Conference on Empirical Methods in Natural Language Processing*, 2022. Accessed: Mar. 07, 2024. [Online]. Available: <http://dx.doi.org/10.18653/v1/2022.emnlp-main.256>
12. W. Lin *et al.*, “PMC-CLIP: Contrastive Language-Image Pre-training using Biomedical Documents,” *arXiv.org*, Mar. 13, 2023. <https://arxiv.org/abs/2303.07240>
13. Y. Lei, Z. Li, Y. Shen, J. Zhang, and H. Shan, “CLIP-Lung: Textual Knowledge-Guided Lung Nodule Malignancy Prediction,” in *Lecture Notes in Computer Science*, 2023, pp. 403–412. [Online]. Available: http://dx.doi.org/10.1007/978-3-031-43990-2_38
14. K. You *et al.*, “CXR-CLIP: Toward Large Scale Chest X-ray Language-Image Pre-training,” in *Lecture Notes in Computer Science*, Cham: Springer Nature Switzerland, 2023, pp. 101–111. Accessed: Mar. 07, 2024. [Online]. Available: http://dx.doi.org/10.1007/978-3-031-43895-0_10
15. M. Tsimpoukelli, J. Menick, S. Cabi, S. M. A. Eslami, O. Vinyals, and F. Hill, “Multimodal Few-Shot Learning with Frozen Language Models,” *arXiv.org*, Jun. 25, 2021. <https://arxiv.org/abs/2106.13884>
16. C. Liu *et al.*, “M-FLAG: Medical Vision-Language Pre-training with Frozen Language Models and Latent Space Geometry Optimization,” *arXiv.org*, Jul. 17, 2023. <https://arxiv.org/abs/2307.08347>

17. X. Gao *et al.*, “COVID-VIT: Classification of Covid-19 from 3D CT chest images based on vision transformer model,” in *2022 3rd International Conference on Next Generation Computing Applications (NextComp)*, Oct. 2022. Accessed: Mar. 07, 2024. [Online]. Available: <http://dx.doi.org/10.1109/nextcomp55567.2022.9932246>
18. Y. Zhang, S.-C. Huang, Z. Zhou, M. P. Lungren, and S. Yeung, “Adapting Pre-trained Vision Transformers from 2D to 3D through Weight Inflation Improves Medical Image Segmentation,” *arXiv.org*, Feb. 08, 2023. <https://arxiv.org/abs/2302.04303>
19. H. Rasheed, M. U. Khattak, M. Maaz, S. Khan, and F. S. Khan, “Fine-tuned CLIP Models are Efficient Video Learners,” in *2023 IEEE/CVF Conference on Computer Vision and Pattern Recognition (CVPR)*, Jun. 2023. Accessed: Mar. 07, 2024. [Online]. Available: <http://dx.doi.org/10.1109/cvpr52729.2023.00633>
20. S. Xie, C. Sun, J. Huang, Z. Tu, and K. Murphy, “Rethinking Spatiotemporal Feature Learning: Speed-Accuracy Trade-offs in Video Classification,” in *Computer Vision – ECCV 2018*, Cham: Springer International Publishing, 2018, pp. 318–335. Accessed: Mar. 07, 2024. [Online]. Available: http://dx.doi.org/10.1007/978-3-030-01267-0_19
21. P. P. Malla, S. Sahu, and A. I. Alutaibi, “Classification of Tumor in Brain MR Images Using Deep Convolutional Neural Network and Global Average Pooling,” *Processes*, vol. 11, no. 3, Feb. 2023, doi: 10.3390/pr11030679.
22. A. Vaswani *et al.*, “Attention Is All You Need,” *arXiv.org*, Jun. 12, 2017. <https://arxiv.org/abs/1706.03762>
23. J. Devlin, M.-W. Chang, K. Lee, and K. Toutanova, “BERT: Pre-training of Deep Bidirectional Transformers for Language Understanding,” *arXiv.org*, Oct. 11, 2018. <https://arxiv.org/abs/1810.04805>
24. G. Alain and Y. Bengio, “Understanding intermediate layers using linear classifier probes,” *arXiv.org*, Oct. 05, 2016. <https://arxiv.org/abs/1610.01644>
25. P. C. C. Coutinho, Y. Berthoumieu, M. Donias, and S. Guillon, “Weakly Supervised Disentanglement with Triplet Network,” in *2023 IEEE International Conference on Image Processing (ICIP)*, Oct. 2023. Accessed: Mar. 07, 2024. [Online]. Available: <http://dx.doi.org/10.1109/icip49359.2023.10222748>
26. A. Dosovitskiy *et al.*, “An Image is Worth 16x16 Words: Transformers for Image Recognition at Scale,” *arXiv.org*, Oct. 22, 2020. <https://arxiv.org/abs/2010.11929>
27. Z. Liu *et al.*, “Swin Transformer: Hierarchical Vision Transformer using Shifted Windows,” in *2021 IEEE/CVF International Conference on Computer Vision (ICCV)*, Oct. 2021. Accessed: Mar. 07, 2024. [Online]. Available: <http://dx.doi.org/10.1109/iccv48922.2021.00986>
28. J. Irvin *et al.*, “CheXpert: A Large Chest Radiograph Dataset with Uncertainty Labels and Expert Comparison,” *Proceedings of the AAAI Conference on Artificial Intelligence*, vol. 33, no. 01, pp. 590–597, Jul. 2019, doi: 10.1609/aaai.v33i01.3301590.
29. J. Yang *et al.*, “MedMNIST v2 - A large-scale lightweight benchmark for 2D and 3D biomedical image classification,” *Scientific Data*, vol. 10, no. 1, Jan. 2023, doi: 10.1038/s41597-022-01721-8.
30. F. Knoll *et al.*, “fastMRI: A Publicly Available Raw k-Space and DICOM Dataset of Knee Images for Accelerated MR Image Reconstruction Using Machine Learning,” *Radiology: Artificial Intelligence*, vol. 2, no. 1, p. e190007, Jan. 2020, doi: 10.1148/ryai.2020190007.
31. J. Zbontar *et al.*, “fastMRI: An Open Dataset and Benchmarks for Accelerated MRI,” *arXiv.org*, Nov. 21, 2018. <https://arxiv.org/abs/1811.08839>
32. J. A. Macdonald, Z. Zhu, B. Konkel, M. A. Mazurowski, W. F. Wiggins, and M. R. Bashir, “Duke Liver Dataset: A Publicly Available Liver MRI Dataset with Liver Segmentation Masks and Series Labels,” *Radiology: Artificial Intelligence*, vol. 5, no. 5, Sep. 2023, doi: 10.1148/ryai.220275.

33. A. E. Kavur, M. A. Selver, O. Dicle, M. Barış, and N. S. Gezer, “CHAOS - Combined (CT-MR) Healthy Abdominal Organ Segmentation Challenge Data,” *Zenodo*, Apr. 11, 2019. <https://zenodo.org/record/3362844>
34. “CMB-CRC,” *The Cancer Imaging Archive (TCIA)*, Nov. 20, 2023. <https://www.cancerimagingarchive.net/collection/cmb-crc/>
35. “CMB-LCA,” *The Cancer Imaging Archive (TCIA)*, Nov. 20, 2023. <https://www.cancerimagingarchive.net/collection/cmb-lca/>
36. “CPTAC-PDA,” *The Cancer Imaging Archive (TCIA)*, Nov. 20, 2023. <https://www.cancerimagingarchive.net/collection/cptac-pda/>
37. “ISPY1,” *The Cancer Imaging Archive (TCIA)*, Nov. 20, 2023. <https://www.cancerimagingarchive.net/collection/ispy1/>
38. “PROSTATE-MRI-US-BIOPSY,” *The Cancer Imaging Archive (TCIA)*, Nov. 20, 2023. <https://www.cancerimagingarchive.net/collection/prostate-mri-us-biopsy/>
39. A. S. Chaudhari *et al.*, “Combined 5-minute double-echo in steady-state with separated echoes and 2-minute proton-density-weighted 2D FSE sequence for comprehensive whole-joint knee MRI assessment,” *Journal of Magnetic Resonance Imaging*, vol. 49, no. 7, Dec. 2018, doi: 10.1002/jmri.26582.